2022 IEEE International Workshop on Metrology for AeroSpace, 27-29 June 2022, Pisa, Italy.
DOI: 10.1109/MetroAeroSpace54187.2022.9856394

RCS Measurements of UAVs and Their Statistical Analysis

Massimo Rosamilia†, Augusto Aubry†, Alessio Balleri#, Vincenzo Carotenuto†, and Antonio De Maio†
†Department of Electrical Engineering and Information Technology,
University of Naples "Federico II", Naples, Italy, I-80125
#Centre for Electronic Warfare, Information and Cyber,
Cranfield University, Defence Academy of the United Kingdom, Shrivenham, SN6 8LA

***Abstract*—This paper deals with Radar Cross Section (RCS) measurements of five small Unmanned Aerial Vehicles (UAVs) in a semi-controlled environment as a function of azimuth aspect angle, polarization, and frequency in the range 8.2-18 GHz. The experimental setup and the data pre-processing, which include coherent background subtraction, range gating procedures, and calibration, are presented. Then, a thorough statistical analysis of the measured RCSs is provided by means of the Cramér–von Mises (CVM) distance and the Kolmogorov–Smirnov (KS) test.**

I. Introduction

Collecting drone data and analyzing their Radar Cross Section (RCS) is a critical step towards the design of appropriate system architectures capable of dealing with these types of targets as well as for the development of an accurate performance prediction of existing algorithms.

In this regard, in [1], the RCSs of small UAVs have been measured for different aspect angles in the frequency interval 8-12 GHz and in VV polarization. The measurements have also been examined using the Inverse Synthetic Aperture Radar (ISAR) method, which provides useful information regarding the components that mostly contribute to the UAV signatures. Besides, in [2], six commercial UAVs have been measured at 15 GHz and 25 GHz for both HH and VV polarizations. The RCS measurement of two off-the-shelf drones in the frequency band 5.8-8.2 GHz has been addressed in [3], and in [4] RCS data of several drones have been collected in the frequency range 26-40 GHz. Some measurements in the Ku radar band have been conducted in [5], whereas, unlike aforementioned references, [6] has presented three-dimensional RCS measurements of a nano-drone from 23 GHz to 25 GHz. A highly accurate UAV RCS simulation has been developed in [7] and the corresponding results compared with those of measurements and simpler simulation approaches. In [8] the RCSs of some nano and micro drones have been collected in the X-band for several elevation angles, and some statistics related to measured RCS data have been provided.

To the best of the authors' knowledge, in the open literature, the statistical analysis of the RCS of commercial drones in a frequency range including the X and Ku radar bands has not been yet addressed. Aimed at filling this gap, this paper presents the statistical analysis of the RCS signatures of five drones: an AscTec Firefly, an AscTec Pelican, a Venom VN10, a Parrot AR.DRONE, and a DJI Matrice 100. The raw RCS data are collected in a semi-controlled environment as a function of frequency (in the interval 8.2-18 GHz), target azimuth aspect angle and polarization. In this respect, a description of the experimental setup and the data pre-processing is provided. Specifically, the pre-processing operations, which include Coherent Background Subtraction (CBS) and range gating procedures, are illustrated with a discussion on the RCS calibration relying on the substitution method. The results are analyzed considering sliding frequency intervals of 200 MHz corresponding to a range resolution of 0.75 m, which allows to model the drones as point-like targets. Finally, a detailed first-order statistical analysis of the measured RCSs is performed by fitting the data with (one- and two- parameters) distributions typically employed to model RCS fluctuations [23], via the minimization of the Cramér–von Mises (CVM) distance between the empirical and the theoretical Cumulative Distribution Functions (CDFs). The Kolmogorov–Smirnov (KS) test is also employed to further assess the goodness-of-fit of the selected distribution.

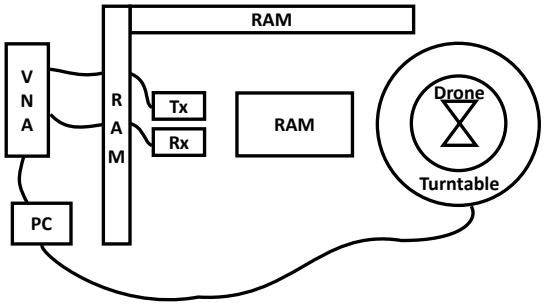

Fig. 1. A notional representation of the experimental setup.

The rest of the paper is organized as follows. Section II presents the experimental setup. In Section III, the statistical behavior of the measured RCSs is analyzed. Finally, conclusions are drawn in Section IV.

II. Experimental Setup

In this section, a description of the experimental setup involved in the measurement campaign is provided along with details on data pre-processing and calibration. The RCS data

TABLE I
SETUP AND ACQUISITION PARAMETERS.

Parameter	Setup 1	Setup 2
Analyzed Frequency Bandwidth	8.2-12.4 GHz	12.4-18 GHz
Azimuth Rotation Step	0.1 degrees	0.1 degrees
Target-antennas Distance	≈ 7.2 m	≈ 3.4 m
Distance from Ceiling	2.71 m	2.71 m
Height above Floor	1.28 m	1.28 m
Range Gating	6.5-7.8 m	1.5-4.6 m
Number of FFT/IFFT Points	400100	400100

has been collected in a laboratory environment using the measurement setup depicted in Fig. 1, which is composed of

- Radar Absorbing Material (RAM) panels to mitigate multipath reflections from the ceiling, walls and floor;
- a 2-port MS46322A Anritsu Vector Network Analyzer (VNA), which measures the frequency response of the illuminated area over a pre-defined bandwidth;
- a LinearX precision turntable with an angular step resolution of (up to) 0.1 degrees, fully controlled remotely from a PC;
- a standard PC to control and synchronize the turntable and the VNA via the Laboratory Virtual Instrument Engineering Workbench (LabVIEW) as well as to store and process the raw data;
- a pair of identical standard horn antennas, one for transmission and the other for reception; they are connected to the two ports of the VNA by means of low-loss coaxial cables and co-located on a tripod. The positions of the antennas have been adjusted with a cross-laser level to steer the antenna boresights at the target. Rotating the antennas allowed data collection for different polarizations.

Before proceeding with the measurements, the VNA has been calibrated using the standard "thru" calibration procedure to provide a measurement setup with a flat frequency response up to the antennas. The LabVIEW scripts have been designed to trigger a turntable step rotation after the data acquisition by the VNA at a specific aspect angle. This has guaranteed collections of frequency responses with a stationary target. In particular, a short time delay has been also included before collecting a new measurement to ensure that the setup was actually stationary after each step rotation.

Although the VNA measured all S-parameters at each frequency [9] of interest, for the considered experiments only S_{21} has been recorded and analyzed. The HH-pol and VV-pol returns from five drones have been measured versus frequency and azimuth aspect angle in the interval 8.2-18 GHz. A summary of the experimental parameters used to collect and analyze the data is reported in Table I, whereas the specifications of the drones are listed in Table II. Note that the employed measurement setup falls in the so-called near-field non-anechoic range scenario [10].

A. Data Pre-processing and Calibration

For each acquisition, a background measurement (obtained in the absence of the drone) has been collected and subtracted coherently in the frequency domain from all the data acquired in the presence of the target. Range-gating has been then applied to the high range resolution background-free profile to further isolate the target response in range from residual multipath reflections which could not be eliminated with the CBS [10], [11]. To this end, a tailored rectangular window, with parameters matched to the drone size and the target-antennas distance (see Table I), has been used. The frequency spectrum of the clean signatures has been then used to extract the point-like target response over a moving bandwidth of 200 MHz, corresponding to a range resolution of 0.75 m. Precisely, the frequency bandwidth is discretized in several overlapping frequency sub-bandwidths of 200 MHz having central frequencies $\{8.3 \text{ GHz} + (i \times 100) \text{ MHz}, i = 0, \ldots, 96\}$ and the data are processed separately in each of them. Therein, the target can be approximated as a point-like reflector (i.e., target scatterers within the range resolution cell) whose power response (i.e., non-calibrated RCS) is extracted as the squared magnitude peak in the time domain. However, in the process of measuring the absolute RCS of a particular target, it is essential to include an accurate RCS calibration step. The substitution method [10] is the most often used calibration procedure for RCS measurements, which involves measuring a calibrating target (with a known RCS) with the same test-bed used to collect data from the target under test [10]. As a result, each measurement related to the RCS of the calibrating target at a given frequency is compared with the theoretical RCS, and the resulting dB difference is utilized to calibrate the target measurements, provided that the test-bed, as well as the system parameters, are stationary. In the performed campaign, a conductive 10 cm diameter sphere has been used to calibrate the drone measurement data.

III. DRONE RCS STATISTICAL BEHAVIOR

The classic approach for evaluating radar detection performance is based on the assumption that the target's RCS fluctuation follows one of the Swerling models I-V [12]. However, as confirmed by some practical cases, amplitude fluctuations do not always comply with the aforementioned models, resulting in a mismatch between the actual and the theoretical radar performance. Indeed, several alternative fluctuation models (e.g., Weibull, Log-normal, shadowed Rice, two-state Rayleigh-chi, just to mention a few) have been proposed in the open literature to cope with this problem [12]–[14]. Using a suitable statistical description for the target RCS behavior enables the accurate prediction of radar detection performance as well as the design of appropriate signal processing architectures. Toward this goal, in this section, the measured RCS signatures of several drones are statistically analyzed by fitting the data with well-known and commonly used distributions (at most bi-parametric), over different frequencies and polarizations. Then, the most appropriate statistical model for each drone RCS collection (in the aspect angle domain) is selected resorting to the CVM distance and the KS test.

TABLE II
MEASURED DRONES SPECIFICATIONS.

Drone	# Rotors	Weight	Width	Depth	Height	Primary Use
AscTec Firefly	6	1600 g	470 mm	430 mm	165 mm	Mapping/Surveying
AscTec Pelican	4	1650 g	360 mm	360 mm	188 mm	Film & Photo/Mapping/Surveying
Venom VN10	4	148 g	290 mm	210 mm	38 mm	Film & Photo
Parrot AR.DRONE 2.0	4	420 g	517 mm	517 mm	127 mm	Film & Photo
DJI Matrice 100	4	2355 g	759 mm	755 mm	205 mm	Film & Photo/Mapping/Surveying

The RCS analysis of the AscTec Firefly is discussed in Subsection III-A, then the other drones are studied in Subsection III-B.

A. *Statistical Analysis of AscTec Firefly RCS*

A detailed analysis of the AscTec Firefly's RCS is provided in this subsection. Before proceeding further, it is worth mentioning that the worst case noise power (averaged over the two polarizations) observed in the measurements, after preprocessing, subband analysis, and calibration, is $N_F \approx -34.5$ dB for the frequency band 8.2-12.4 GHz, and $N_F \approx -44.5$ dB for the interval 12.4-18 GHz. Given the noise level N_F, an estimate of the measurements SNR in a given frequency bin, which provides insights on the measurement accuracy [15], is given by the ratio between the target RCS and N_F, i.e., it can be practically computed as $SNR(f,p) = \hat{\sigma}(f,p)/N_F$, with $\hat{\sigma}(f,p)$ the measured RCS of the target at frequency f and polarization p. For the case at hand, apart for a few outliers, the SNR is in the order of 20 dB.

As to the RCS, Fig. 2 displays both the mean and standard deviation values (with respect to aspect angle) versus frequency, with reference to both HH and VV RCS acquisitions. Remarkably, similar average RCS values are obtained in both the HH and VV polarizations, in agreement with [1]. The plots also reveal that, for a given frequency bin, the standard deviation of the measured RCS is about 15 dB, which might be attributed to the presence of a few major scatterers whose interaction significantly changes with aspect angles. This behavior is supported by Fig. 3, which illustrates the RCS of the drone in polar coordinates (at varying azimuth angle) for HH polarization and different central frequencies, i.e., 9.5 GHz, 10.7 GHz, 14.1 GHz, and 15.9 GHz. The figure highlights that the RCS is characterized by a fast fluctuation in angle. As already said, this behavior is mainly determined by the composition of the dominant scatterers returns.

Let us now focus on the first-order statistical analysis. Since the drone RCS strongly changes with aspect angle, it appears reasonable the exploitation of a statistical model to describe the target fluctuation and accurately predict radar detection performance. Inspired by previous studies on target RCS fluctuation statistics, in this paper the distributions (at most bi-parametric) reported in Table III are considered to model the RCS of the AscTec Firefly. In the table, $\Gamma(x)$, $\gamma(a,b)$, and $\mathrm{erf}(x)$ indicate the Gamma, the incomplete Gamma, and the error functions, respectively.

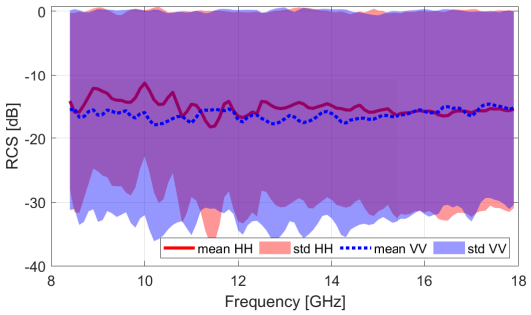

Fig. 2. Mean values of AscTec Firefly's RCS versus frequency for HH and VV polarizations (solid and dashed lines, respectively). The top (bottom) border of the shaded area represents the mean value plus (minus) standard deviation.

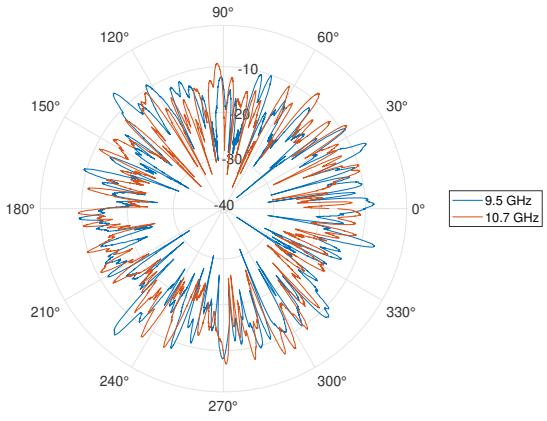

(a)

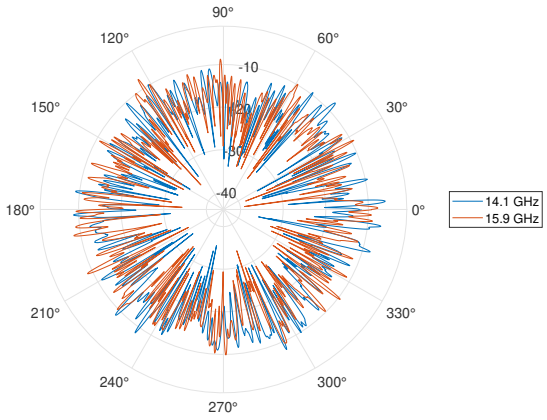

(b)

Fig. 3. Polar plot of AscTec Firefly RCS [dBsqm] for HH polarization in the frequency bin with central frequency: (a) 9.5 GHz (blue curve) and 10.7 GHz (red curve), (b) 14.1 GHz (blue curve) and 15.9 GHz (red curve).

TABLE III
CDFs OF THE CONSIDERED MODELS.

Distribution	CDF	Parameter 1	Parameter 2	Mean
Exponential	$F(x;\lambda) = 1 - e^{-\lambda x}, x \geq 0$	$\lambda > 0$, rate	-	$\mu = 1/\lambda$
Gamma	$F(x;\alpha,\beta) = \frac{1}{\Gamma(\alpha)}\gamma\left(\alpha, \frac{x}{\beta}\right), x \geq 0$	$\alpha > 0$, shape	$\beta > 0$, scale	$\mu = \alpha\beta$
LogNormal	$F(x;\chi,\sigma) = \frac{1}{2}\left[1 + \text{erf}\left(\frac{\ln x - \chi}{\sigma\sqrt{2}}\right)\right], x > 0$	$\chi \in (-\infty, +\infty)$	$\sigma > 0$	$\mu = e^{\chi + \frac{\sigma^2}{2}}$
Weibull	$F(x;a,b) = 1 - e^{-(x/a)^b}, x \geq 0$	$a \in (0, +\infty)$, scale	$b \in (0, +\infty)$, shape	$\mu = a\Gamma(1 + 1/b)$

The fitting of the above-mentioned distributions with the data is performed considering the RCS measurements for different aspect angles at a given frequency f and in a polarization $p = \{HH, VV\}$. Formally, the parameter vector of the distributions is determined as a solution to the following optimization problem

$$\widehat{\boldsymbol{\theta}}(f,p) = \arg\min_{\boldsymbol{\theta}} CVM(\hat{\boldsymbol{\sigma}}(f,p), F(x;\boldsymbol{\theta})) \tag{1}$$

where $F(x;\boldsymbol{\theta})$ is the CDF of the distribution under test, $\boldsymbol{\theta}$ denotes the distributional parameters, $\hat{\boldsymbol{\sigma}}(f,p) = [\hat{\sigma}_1(f,p), \hat{\sigma}_2(f,p), \ldots, \hat{\sigma}_n(f,p)]^{\mathrm{T}} \in \mathbb{R}^n$, with $n = 3600$, is the vector of the measured/observed RCS, and [16]

$$CVM(\hat{\boldsymbol{\sigma}}(f,p), F(x;\boldsymbol{\theta})) = \sqrt{\frac{1}{12n} + \sum_{i=1}^{n}\left[\frac{2i-1}{2n} - F(\hat{\sigma}_i(f,p);\boldsymbol{\theta})\right]^2} \tag{2}$$

is the CVM distance. The optimization problem in (1) is tackled by means of the iterative algorithm proposed in [17] which is implemented in MATLAB with the function *fminsearch*, using as initial estimates of the distributional parameters those obtained via the MATLAB function *fitdist*. The average CVM distances between the optimally fitted (according to (1)) distributions and the empirical CDF for different frequencies are reported in the first column of Table IV. Inspection of the table reveals that the Gamma CDF in general achieves the lowest average CVM distance from the measured data, whereas the Weibull distribution ranks second. Hence, to confirm the quality of the Gamma model to faithfully describe the collected data, a KS test is performed [16], [18]. This is a non parametric statistical procedure which can be used to assess the goodness-of-fit between the empirical and the theoretical RCS distributions, i.e., it tests the simple hypothesis

$$\mathcal{H}_0 : \hat{\sigma}_i(f,p) \text{ has the CDF } F(x;\widehat{\boldsymbol{\theta}}(f,p)),\ p = \{HH, VV\}. \tag{3}$$

In a nutshell, the KS test tackles the hypothesis testing problem (3) by comparing a threshold with the largest absolute difference between the empirical CDF of the data and the theoretical one. Formally,

$$D_n(f,p) \underset{\mathcal{H}_0}{\overset{\mathcal{H}_1}{\gtrless}} \gamma(\alpha_{KS}) \tag{4}$$

where

$$D_n(f,p) = \sup_{\hat{\sigma}_i(f,p) \in \hat{\boldsymbol{\sigma}}(f,p)} \left|\hat{F}(\hat{\sigma}_i(f,p)) - F(\hat{\sigma}_i(f,p);\widehat{\boldsymbol{\theta}}(f,p))\right| \tag{5}$$

with $\hat{F}(\hat{\sigma}_i(f,p))$ the empirical CDF at a given frequency and polarization of the measured RCS values (for different aspect angles) collected in the vector $\hat{\boldsymbol{\sigma}}(f,p)$, whereas $\gamma(\alpha_{KS})$ is the decision threshold (which does not depend on the tested distribution) set to ensure the desired significance level α_{KS}. Besides, the implementation of (4) is tantamount to comparing the p-value of $D_n(f,p)$, under the null hypothesis, with α_{KS} [19]. Considering a significance level $\alpha_{KS} = 0.01$, the outcomes of the KS tests unveils that, regardless of frequency and polarization, the $\mathcal{H}_0$ hypothesis cannot be rejected.

Finally, Fig. 4 concludes this subsection with the analysis of the Gamma parameters obtained with the fitting procedure. In particular, Fig. 4(a) compares the sample mean of the measured RCS with the first moment of the fitted Gamma distribution. The results show that Gamma expectation is very close to the mean RCS $\tilde{\sigma}_p,\ p = \{HH, VV\}$ of the drone. The shape parameter of the optimally fitted Gamma is examined in Fig. 4(b) versus the frequency. A close examination of the figure reveals that the shape parameter is relatively close to 1, indicating that the RCSs can be well represented using a statistical distribution close to an Exponential (Swerling I-II) model. However, based on the results shown in Table IV, a plain Exponential distribution is unable to fully predict the behavior of the measured data, and a bi-parametric distribution, i.e., the Gamma, appears necessary to better capture the data statistical properties.

B. Statistical Analysis of Others Drones RCS

In this subsection, the statistical analysis is conducted on the collected RCSs of the other tested drones (see Table II). Fig. 5 shows the mean and standard deviation values of the RCS versus frequency for HH and VV polarizations. Like the results obtained for the AscTec Firefly (see Fig. 2), the considered drones achieve similar RCS values in both HH and VV polarizations. Moreover, large fluctuations in the RCS values can be observed, with a standard deviation in the order of 10 dB for the AscTec Pelican and DJI Matrice 100 (Figs. 5(a) and 5(d)) and 20 dB for the Venom VN10 and the Parrot AR.DRONE 2.0 (Figs. 5(b) and 5(c)). As to the statistical analysis, Table IV reports the mean values (over the frequency) of the CVM distances computed between the empirical and theoretical CDFs of the measured RCSs in both HH and VV polarizations. Interestingly, the Gamma model is still able to achieve the lowest average CVM distance in almost all the scenarios, with some exceptions where Weibull distribution prevails over the others (see for instance the case of Asctec

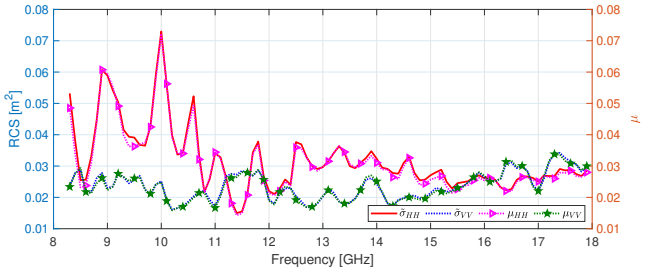

(a)

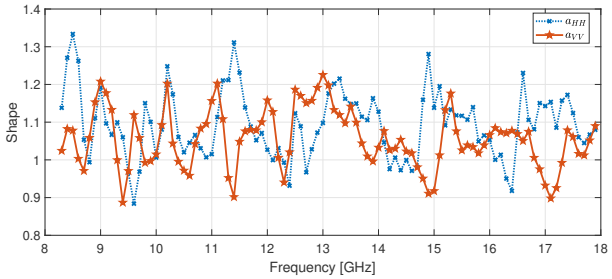

(b)

Fig. 4. Analysis of the Gamma distribution's parameters versus frequency, fitted with the RCS measurements of AscTec Firefly. (a) Comparison between the mean RCS values and the expectation of the fitted Gamma distribution versus frequency for HH and VV polarization; (b) Gamma shape parameter values versus frequency.

Pelican in HH or Venom VN10 in VV). However, under these specific instances, the mean CVM distances achieved by the Gamma and the Weibull model are relatively close. Moreover, unlike the Weibull, the Gamma fluctuation law enables a quite simple and closed-form analytical evaluation of the detection performance [14].

Fig. 6 shows the shape parameter values of the fitted Gamma versus frequency for both polarizations. For most cases, the Gamma shape parameter is close to 1, underlining that the measured RCS first-order statistics are not far from an Exponential-like behavior. The only exception which is worth of a further investigation is the AscTec Pelican. As a matter of fact, Fig. 6(a) reveals that for the frequency band 10.2-10.8 GHz and VV polarization, the Gamma shape parameter is close to 2, meaning that the fluctuation follows a chi-squared distribution with 4 degrees of freedom. Remarkably, this latter distribution (used in the Swerling 3 and 4 models) is typically employed to model targets composed of scatterers of similar strength plus one dominant scatterer, with the latter having RCS $1+\sqrt{2}\sigma_o$, where σ_o is the sum of RCS of the randomly distributed equal-strength scatterers [12].

IV. Conclusion

This paper has considered the statistical analysis of the RCS of small UAVs collected in a semi-controlled environment as a function of frequency, angle, and polarization. Specifically, five drones of different sizes and characteristics have been measured in the frequency range 8.2-18 GHz, and their RCSs have been analyzed considering first order statistics over a moving bandwidth of 200 MHz. The statistical analysis has been performed checking the adequacy of some distributions (at most bi-parametric) to describe the first-order RCS statistics. The results have highlighted that, in the considered frequency bands, the RCSs of the drones assume quite small values and are characterized by strong fluctuations in angle. Besides, from a statistical standpoint, the Gamma distribution proved capable of modeling such measurement variability, characterized, in the majority of cases, by Exponential-like fluctuations. Precisely, the RCS variability can be usually described using Gamma shape parameter values close to 1. Therefore, the developed analysis can provide useful insights toward an accurate prediction of the radar detection performance for the considered targets.

References

[1] M. Pieraccini, L. Miccinesi, and N. Rojhani, "RCS measurements and ISAR images of small UAVs," *IEEE Aerosp. Electron. Syst. Magazine*, vol. 32, no. 9, pp. 28–32, 2017.

[2] M. Ezuma, C. K. Anjinappa, M. Funderburk, and I. Guvenc, "Radar cross section based statistical recognition of UAVs at microwave frequencies," *IEEE Trans. Aerosp. Electron. Syst.*, vol. 58, no. 1, pp. 27–46, 2022.

[3] A. Herschfelt, C. R. Birtcher, R. M. Gutierrez, Y. Rong, H. Yu, C. A. Balanis, and D. W. Bliss, "Consumer-grade drone radar cross-section and micro-doppler phenomenology," in *2017 IEEE Radar Conference (RadarConf)*, 2017, pp. 0981–0985.

[4] V. Semkin, J. Haarla, T. Pairon, C. Slezak, S. Rangan, V. Viikari, and C. Oestges, "Analyzing radar cross section signatures of diverse drone models at mmWave frequencies," *IEEE Access*, vol. 8, pp. 48958–48969, 2020.

[5] J. Ochodnický, Z. Matousek, M. Babjak, and J. Kurty, "Drone detection by Ku-band battlefield radar," in *2017 International Conference on Military Technologies (ICMT)*, 2017, pp. 613–616.

[6] A. Balleri, "Measurements of the radar cross section of a nano-drone at K-band," in *2021 IEEE 8th International Workshop on Metrology for AeroSpace (MetroAeroSpace)*, 2021, pp. 283–287.

[7] P. J. Speirs, A. Murk, M. Renker, P. Wellig, and U. Aulenbacher, "High-detail simulations of consumer-grade UAV RCS signatures, and comparisons against measurements," *STO-MP-MSG-SET-183*.

[8] P. Sedivy and O. Nemec, "Drone RCS statistical behaviour," *STO-MP-MSG-SET-183*, 2021.

[9] Calibration and Measurement Guide, *ShockLine MS46122A/B, MS46131A, ME7868A, and MS46322A/B Series Vector Network Analyzer*, Number 10410-00336. Anritsu Company, 2021.

[10] IEEE, "Recommended practice for radar cross-section test procedures," *IEEE Std 1502-2020 (Revision of IEEE Std 1502-2007)*, pp. 1–78, 2020.

[11] M. F. Sundermeier and D. Fischer, "Compact radar cross-section measurement setup and performance evaluation," *Advances in Radio Science*, vol. 19, pp. 147–152, 2021.

[12] M. A. Richards, J. A. Scheer, and W. A. Holm, *Principles of Modern Radar: Basic Principles, Volume 1*, Institution of Engineering and Technology, 2010.

[13] D. A. Shnidman, "Expanded swerling target models," *IEEE Trans. Aerosp. Electron. Syst.*, vol. 39, no. 3, pp. 1059–1069, 2003.

[14] A. De Maio, A. Farina, and G. Foglia, "Target fluctuation models and their application to radar performance prediction," *IEE Proceedings-Radar, Sonar and Navigation*, vol. 151, no. 5, pp. 261–269, 2004.

[15] "IEEE recommended practice for radar cross-section test procedures," *IEEE Std 1502-2020 (Revision of IEEE Std 1502-2007)*, pp. 1–78, 2020.

[16] R. D'Agostino and M. Stephens, *Goodness-of-Fit Techniques*, New York: Marcel Dekker, 1986.

[17] J. A. Nelder and R. Mead, "A simplex method for function minimization," *The computer journal*, vol. 7, no. 4, pp. 308–313, 1965.

[18] W. W. Daniel, *Applied Nonparametric Statistics*, Duxbury advanced series in statistics and decision sciences. PWS-KENT Pub., 1990.

[19] R. Simard and P. L'Ecuyer, "Computing the two-sided kolmogorov-smirnov distribution," *Journal of Statistical Software*, vol. 39, pp. 1–18, 2011.

TABLE IV
MEAN CVM DISTANCES BETWEEN EMPIRICAL AND THEORETICAL CDF.

	mean CVM distance HH / VV				
Distribution	**AscTec Firefly**	**AscTec Pelican**	**Venom VN10**	**Parrot AR.DRONE 2.0**	**DJI Matrice 100**
Exponential	0.93 / 0.73	1.21 / 1.43	1.17 / 1.08	0.93 / 0.99	0.85 / 0.77
Gamma	**0.59 / 0.49**	0.73 / **0.66**	**0.62** / 0.69	**0.66 / 0.57**	**0.62 / 0.55**
LogNormal	1.11 / 1.37	1.09 / 1.15	1.26 / 1.32	1.06 / 1.21	0.98 / 1.04
Weibull	0.63 / 0.50	**0.67** / 0.68	0.65 / **0.66**	0.67 / 0.58	0.64 / 0.58

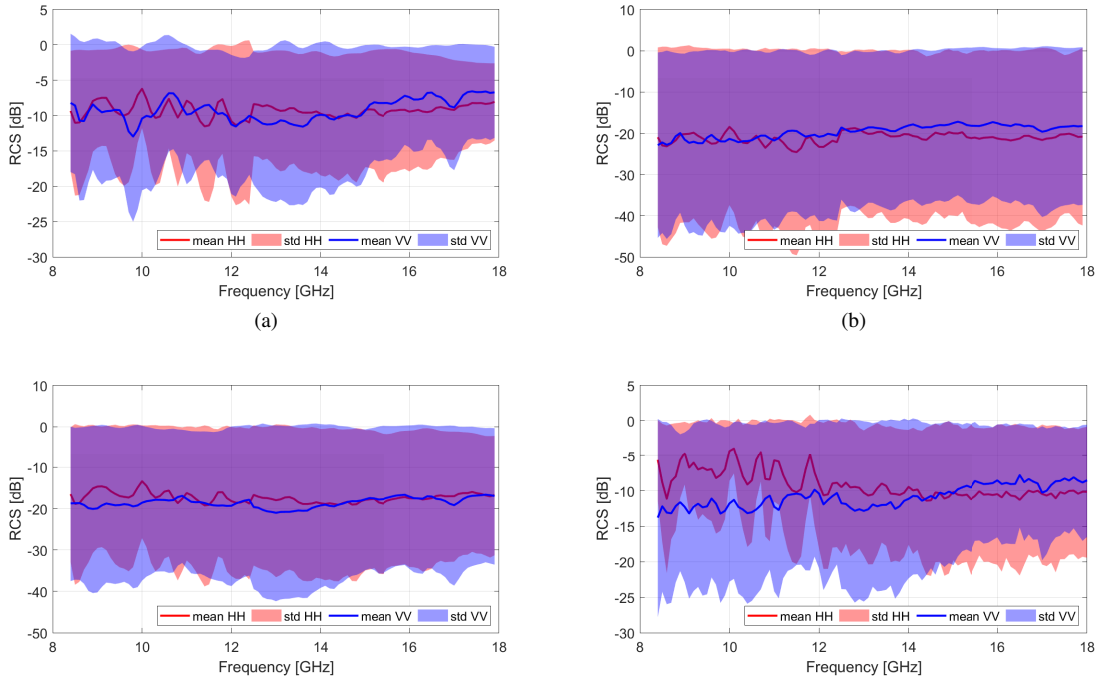

Fig. 5. RCS mean and standard deviation values versus frequency for a) AscTec Pelican, b) Venom VN10, c) Parrot AR.DRONE 2.0, d) DJI Matrice 100.

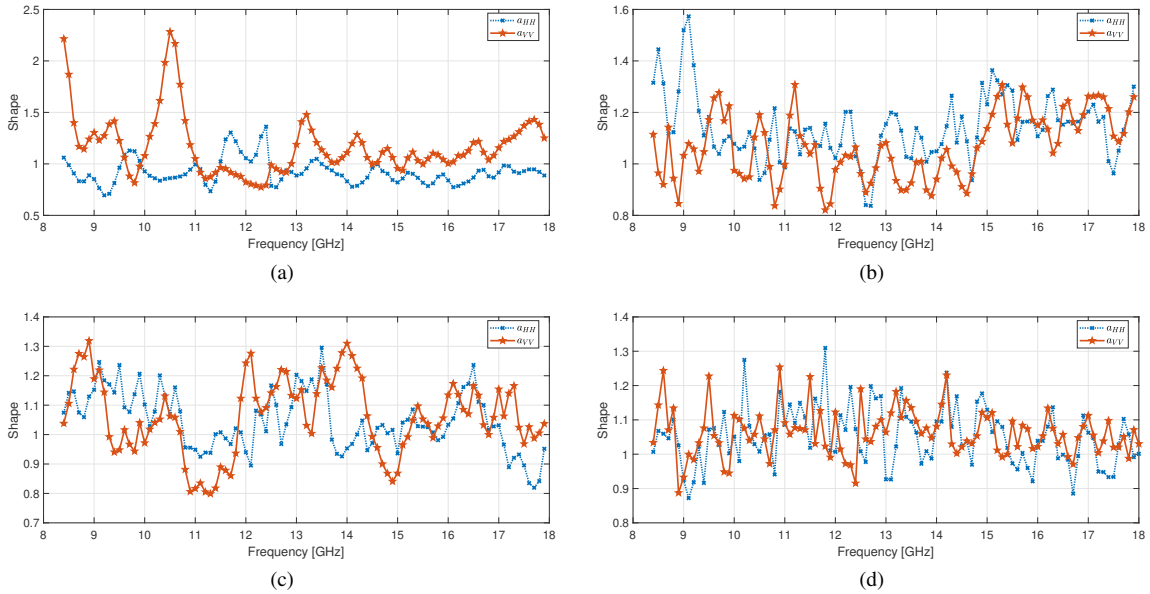

Fig. 6. Shape parameter values of the Gamma distribution fitted with the RCS data of a) AscTec Pelican, b) Venom VN10, c) Parrot AR.DRONE 2.0, d) DJI Matrice 100, versus frequency in HH and VV polarization.